Neutrino Oscillations at the Icecube Neutrino Observatory

DESY Summer Student Project Report 2021
26^{th} July to 10^{th} September, 2021

Submitted by:
Ms. Vaibhavi B Gawas
Department of Physics,
Indian Institute of Technology Madras, Chennai, India

Supervised by:
Alexander Trettin, Leander Fischer, Dr. Summer Blot
Low Energy Neutrino Physics Group,
DESY, Zeuthen, Germany

Abstract

The Icecube Neutrino Observatory is one of the leading experiments in the field of neutrino physics. Over last ten years the detector has considerably improved the constraints on the mixing parameters associated with the atmospheric neutrino oscillations.
This work briefly introduces the theoretical basis of neutrino oscillations, with focus on the matter effects and then the atmospheric neutrinos. The icecube detector is also discussed. Finally, the analysis of monte-carlo simulated reconstructed energy and zenith-angle of the atmospheric ν_e, ν_μ, ν_τ in the energy range of 6.3 to 158.49 GeV and passing through the earth (i.e the cosine(zenith angle between -1.0 to 0.1) is presented and discussed. The are filled in 2D histograms of energy and cosine of zenith angle using the oscillated weights and used to identify regions of neutrino appearance and disappearance. The dependence of energy and zenith angle distributions on track-like signatures of the events is also presented.

Contents

Acknowledgement

I am very pleased to thank Alexander Trettin and Leander Fischer for guiding me through each step of this project and patiently dedicating their own time. I would express my gratitude to our group leader of Low Energy Neutrino Oscillations group, Dr. Summer Blot for her supervision. I would also thank Dr. Wing Yan Ma for her guidance during this summer. A thank you to Dr. Prabhat Pujahari and Dr. L Sriramkumar who supported my application to the DESY Summer Student Program.

1 Introduction

In the Standard Model , the neutrinos are the massless, electrically neutral, spin-1/2 fermions, interacting via the weak-force or exchange of W and Z bosons. The existence of neutrinos was first proposed by Wolfgang Pauli to explain the electron energy spectrum in the beta-decay that seemed to violate the energy conservation law [10]. Figure 1 describes these in more details.

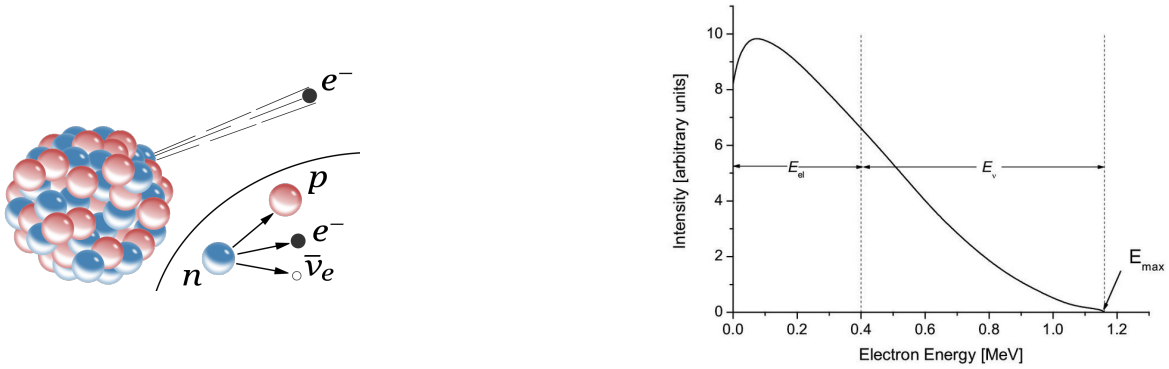

Figure 1: Figure on left side shows the decay of neutron into a proton, electron and anti-neutrino. This is the beta decay process, in which the electron energy spectrum obtained is as given in the right panel. The non-interacting particle (neutrino) that would carry away the interaction energy, was proposed to explain the decrease in the intensity of the given spectrum.

There are three neutrino favors $(\nu_e, \nu_\mu, \nu_\tau)$ corresponding to three leptons of SM, and interacting only via gravity and weak force. Their interactions through the weak force can be summarised through the feynman diagrams given in the following Figure 2

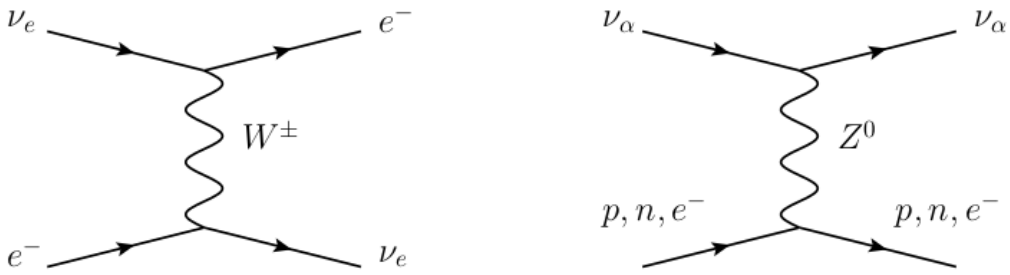

Figure 2: The figure in the left panel shows the neutrino-lepton interaction via exchange if the W boson, also known as charged current interaction. It is possible to identify the neutrino flavor by detecting its corresponding lepton in this type of interaction. The right panel shows the neutral current interaction of a neutrino. In this the neutrino scatter away from the matter particles such as protons, neutrons or leptons via exchange of the Z boson.

In the early 1950s the Poltergeist experiment by F Reines and C Cowan was the first experiment to detect free neutrino interactions [5]. Following which the Homestake experiment by Davis Raymond and John Bahcall was setup to observe the solar neutrinos emitted by nuclear fusion processes in Sun. Through number of error corrections and several checks, the homestake experiment could observe only 1/3 of the theoretically predicted solar neutrinos[4] . At this time the solar model was robust

and extremely well formalised, that the theoretical prediction could not be wrong, neither were the experimental results incorrect. Following this discrepancy in theoretical model and experimental facts, Pontecorvo, Maki, Nakagawa and Sakata speculated that neutrinos could change flavor or oscillate between different flavors if they had mass and evidently the mass eigenstates. [9][11]. The theory of neutrino with non-zero mass is now described under 'beyond standard model' domain.

The phenomena of Neutrino oscillations was observed and confirmation of the existence of neutrino masses was provided through the solar electron neutrino deficit measured by the Sadbury neutrino observatory (SNO) group [6] and the disappearance of atmospheric muon neutrinos observed at Super Kamiokande Observatory [3]. Arthur McDonald and Takaaki Kajita who led the SNO and Super-Kamiokande group respectively were awarded the Nobel prize in physics in 2015.

2 Neutrino Oscillations

Neutrino oscillations belongs to the beyond standard model domain, and breaks the 'massless-neutrinos' assumption of the standard model. In neutrino oscillations the three quantum flavor states exists as a superposition of three different quantum mass eigenstates. There is no equivalent classical or quantum phenomena observed (the kaon-antikaon oscillations exists but are described through a different phenomenology).

After the confirmation of neutrino masses and oscillations, various experiments verified the predictions describing neutrino oscillations in different mediums and under different conditions. The oscillations are described in terms of the probability of one neutrino flavor oscillating into another. The mathematical formalism of deriving such probabilities is described below.

2.1 Mathematical Formalism

The neutrino oscillations are quantum mechanical and described by associated quantum probabilities. The mathematical formalism is characterised by the PMNS matrix (U) that defines the oscillations between three neutrino flavors in terms of the three different mass eigenstates as given.
The PMNS matrix is characterised by three 'mixing angles' (i.e θ_{12}, θ_{23} and θ_{13}). The matrix also includes a Charge parity violation (CP)-phase that has not yet been well-established and depends largely on whether neutrinos are Dirac or Majorana fermions.

The probability that a neutrino that started in one flavor state (Say ν_α oscillates to another flavor state (Say ν_β) can be calculated as followed.

The flavor eigenstates are expressed in the basis of mass eigenstates and vice versa.

$$|\nu_\alpha\rangle = U^*_{\alpha k} \, |\nu_k\rangle$$

$$|\nu_k\rangle = U_{\alpha k} \, |\nu_\alpha\rangle$$

where α is ν_e, ν_μ or ν_τ, and k = 1,2,3 (the three mass eigenstates) $U_{\alpha k}$ is the PMNS matrix given as;

$$U_{\alpha k} = \begin{pmatrix} U_{e1} & U_{e2} & U_{e3} \\ U_{\mu 1} & U_{\mu 2} & U_{\mu 3} \\ U_{\tau 1} & U_{\tau 2} & U_{\tau 3} \end{pmatrix} = \begin{pmatrix} 1 & 0 & 0 \\ 0 & c_{23} & s_{23} \\ 0 & -s_{23} & c_{23} \end{pmatrix} . \begin{pmatrix} c_{13} & 0 & s_{13} e^{-i\delta_{CP}} \\ 0 & 1 & 0 \\ -s_{13} e^{i\delta_{CP}} & 0 & c_{13} \end{pmatrix} . \begin{pmatrix} c_{12} & s_{12} & 0 \\ -s_{12} & c_{12} & 0 \\ 0 & 0 & 1 \end{pmatrix}$$

The amplitude of the oscillation as a function of time (t) and Hamiltonian (H_0) of the system can then be constructed as:

$$\begin{aligned} A_{\nu_\alpha \to \nu_\beta}(t) &= \langle \nu_\beta | \nu(t) \rangle \\ &= \langle \nu_\beta | \, e^{-iH_0 t} \, | \nu_\alpha \rangle \\ &= \Sigma_k U^*_{\alpha k} e^{-iE_k t} \, \langle \nu_\beta | \nu_k \rangle \\ &= \Sigma_k U^*_{\alpha k} U_{\beta k} e^{-iE_k t} \end{aligned} \tag{1}$$

The square of the amplitude evidently leads to probability,

$$\begin{aligned} &P(\nu_\alpha \to \nu_\beta(t)) = \\ &|A_{\nu_\alpha \to \nu_\beta}(t)|^2 = \Sigma_{kj} U^*_{\alpha k} U_{\beta k} U_{\alpha j} U^*_{\beta j} e^{-i(E_k - E_j)t} \end{aligned}$$

Writing E_k and E_j in terms of the mass squared difference and t = L (v c = 1) gives,

$$P_{\nu_\alpha \to \nu_\beta}(t)) = \Sigma_{kj} U^*_{\alpha k} U_{\beta k} U_{\alpha j} U^*_{\beta j} e^{-i \frac{\Delta m^2_{kj}}{2E} L}$$

These leads to,

$$P_{\nu_\alpha \to \nu_\beta}(L, E)) = \delta_{\beta\alpha} - 4\Sigma_{k>j} R(U^*_{\alpha k} U_{\beta k} U_{\alpha j} U^*_{\beta j}) \sin^2\left(\frac{\Delta m^2_{kj}}{4E} L\right) \pm 2\Sigma_{k>j} I(U^*_{\alpha k} U_{\beta k} U_{\alpha j} U^*_{\beta j}) \sin\left(\frac{\Delta m^2_{kj}}{2E} L\right)$$

The amplitude of probability, as can be seen from equation given above, depends on the values of the mixing angle (PMNS) matrix. While the frequency of the oscillations is function of the energy, the mass squared difference and the length of the track. This dependence of the mixing angles, mass suared difference and energy is described more precisely in the following figure number 3.

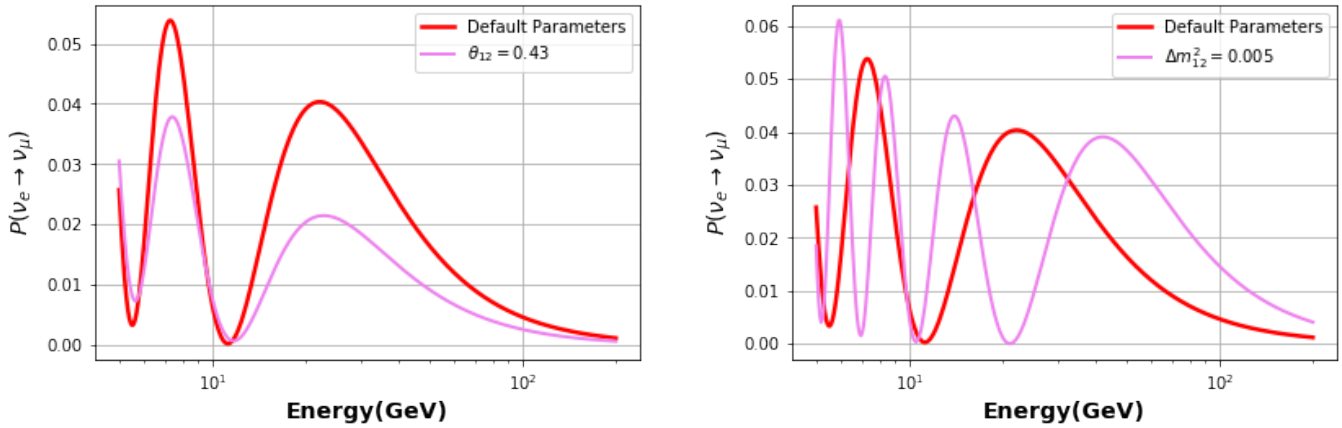

Figure 3: Figure on left side shows how the amplitude of the probability oscillogram changes with respect to the mixing angle. While the other figure shows how the frequency of the probability oscillation varies for a change in mass squared difference. Both graphs shows the oscillations for neutrinos in vacuum, calculated at a distance of L = 10000 Km. All other mixing parameters and mass squared difference are set to the default values.

The above probability accounts for the oscillation in the vacuum. In other mediums interaction of neutrinos with their corresponding leptons or with nucleons can alter the total Hamiltonian. The

evolution of the probabilities is then affected by the new Hamiltonian. Mass-squared differences being dependent on the Hamiltonian of the system are bound to change in different mediums (vacuum, constant-density, earth, atmosphere etc). This changes reflect through a change in oscillation frequency as well as amplitude. Thus the calculation of the new Hamiltonian subsequently leads to new oscillation probabilities. The changes constitute the matter effects discussed in the next subsection.

2.2 Matter Effects

Although neutrinos rarely interact with matter, the number of targets available inside matter medium is enormous. The targets create an effective potential leading to coherent forward scattering[13]. The neutral current interactions are constant across the three flavors and brings up only phase factor. But the charged current interactions which only involves the electron neutrinos leads to an uneven phase difference between the three flavors.
The Hamiltonian due to matter effects is then given by,

$$\mathrm{H} = \mathrm{H_0} + \mathrm{H_I}$$

where $\mathrm{H_0}$ is the Hamiltonian in vacuum, and $\mathrm{H_I}$ is the Hamiltonian due to interactions with matter. The potential associated with $\mathrm{H_I}$ is the V_{CC} given as,

$$\mathrm{V_{CC}} = \pm\sqrt{2}\mathrm{G_F n_e}(x),$$

where $\mathrm{G_F}$ is the fermi constant and $\mathrm{n_e(x)}$ is the electron number density along the path of propagation. This evidently leads to,

$$\mathrm{H_I}\,|\nu_\mathrm{e}\rangle = \mathrm{V_C C}\,|\nu_\mathrm{e}\rangle$$

The modified Hamiltonian leads to change in the oscillation parameters and the probability for a simplified two-neutrino case can be expressed as;

$$\mathrm{P}_{\nu_\alpha \to \nu_\beta}(\mathrm{L,E})) = \sin^2(2\theta_\mathrm{M})\sin^2(\frac{\Delta \mathrm{m^2_M}}{4\mathrm{E}}\mathrm{L})$$

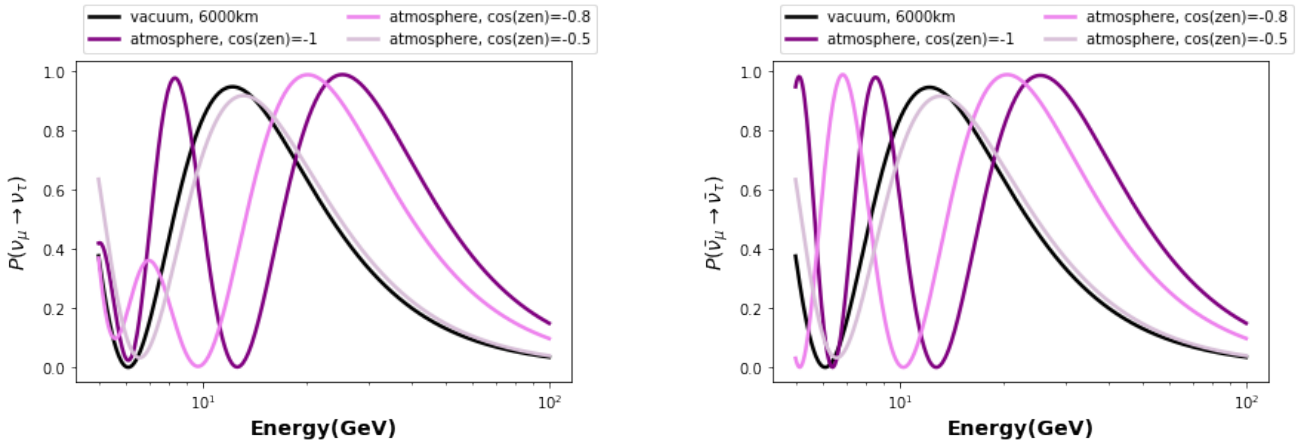

Figure 4: The figure on left describes the probability of muon neutrinos oscillating into tau neutrinos, while the right panel shows the case of anti-muon and anti-tau neutrinos. A sharp peak for cosine(zenith) equal to -0.8 and -1 can be observed at lower energy in panel 2, as a distinguishing feature between neutrino and anti-neutrino case. The matter effects are discussed below.

The figure 4 shows the effect on matter interaction on the atmospheric neutrinos passing through earth. The neutrinos at cosine(zenith) equal to -0.8 and -0.1 pass through the core of the earth where the high density maximises the matter effects. The neutrinos with cosine(zenith) equal to 0.5 avoids the core and therefore its oscillogram lies quite close to that of neutrinos passing through vacuum through distance of 6000km (equivalent to radius of earth). The shift in probabilities due the the matter effects can be therefore clearly observed.

The case of deriving probabilities in case of the three flavors is much more complicated and not presented in this report.

2.3 Atmospheric Neutrinos

The earth's atmosphere is constantly bombarded by the cosmic rays from space. When the cosmic rays consisting of the proton, helium (or sometimes heavier element) nuclei strikes atmospheric atoms and molecules they form a cascade or showers of particles. Most of the particles in such a cascade consists of the short lived pions. The charged pions with the mean lifetime of $2 \times 10^{-8} s$ decays into muon (antimuon) and muon-antineutrino (muon-neutrino). The muons are also unstable particles and decay into electron, electron anti-neutrino, and muon-neutrino with mean lifetime of $2 \times 10^{-6} s$. Therefore about 2/3 of the neutrino fraction is expected to be of muon-neutrinos, and remaining the electron-neutrinos. [7].

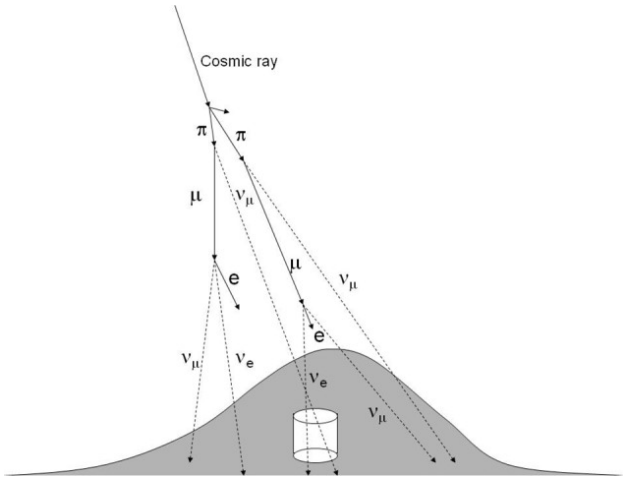

Figure 5: The cosmic rays interacting with earth's atmosphere produces the cascade of particles that consists of neutrinos, roughly 15km above the earth's surface.

3 Detector

The icecube deepcore detector is a Cherenkov detector for the detection of low energy neutrinos (1 GeV to 1 TeV). The deepcore has measured and continues towards precision measurement of disappearance of atmospheric muon neutrinos and appearance of the tau neutrinos, in a not yet well explored energy range. The icecube detector consists of 5160 digital optical modules (DOMs) and each of the DOM has 10 photo-multipliers tubes (PMTs), plus the electronic readout and calibration devices. The modules are set in 86 vertical strings; out of which 8 strings of high quantum efficiency are located at the bottom centre, forming the deepcore detector for atmospheric neutrinos.
The secondary particles created via neutrino interaction and travelling faster than the speed of light in the given medium, emit the Cherenkov radiation(photons) which is detected and reconstructed from the photomultipliers. The Cherenkov photons are detected and amplified by the digital optical

modules (DOMs) and photomultipliers.[12][8].
Icecube deepcore has precisely measured ν_μ disappearance[1] and ν_τ appearance[2] in an energy range not well constrained by any other experiments. θ_{23} and Δm^2_{23} are the parameters constrained by observation from Icecube deepcore experimental measurements.

4 Simulation and Data

4.1 Monte Carlo Data

The monte carlo simulated re-verification data sample of the atmospheric neutrinos is discussed in this section. 1D-histograms for reconstructed and true energy and zenith angle parameters are constructed. 2D-histograms of energy and cosine(zenith) distribution are filled to observed the regions of disappearance of the electron and muon neutrinos and for appearance of the tau neutrinos.
Following is the list of the selection criteria applied to retrieve the required values of the re-constructed energy, reconstructed cosine of the zenith angle, true energy and true zenith angle and finally the plots with different GBM-PID cuts (see the following table too) are also discussed. All the events are weighted with the currently known atmospheric neutrino oscillation parameters.
Combining all the charged and neutral current events about 4,563,713 muon neutrinos were detected. Out of which 281,613 (6.1 %) of the events pass through the selection criteria for the analysis. For electron neutrinos total of 1,995,256 neutrinos were recorded while from tau neutrinos were 2,045,091. From this 39,104 (2.16 %) number of electron neutrinos and 46,393 (2.3 %) number of tau neutrinos passed through the criteria given below.

Selection criteria	Description
GBM PID value > 0.55	Takes in the most track like signatures from the data. 0 represents not at all track like, while 1 is for most track-like signal.
cos(zenith angle) < 0.1	Removes events which come from above the detector, without passing through the earth.
Reconstructed energy between 6.31 and 158.49 GeV	The energy range required for the analysis.
Probability(ν) > 0.97	For selecting events that are most likely neutrinos and not atmospheric muons.
Reduced chi^2 < 50	Good fit events as per their measured chi^2 values
Successful fit condition	Filters events where the reconstruction is indeed successful.
n_{outer} <8 and $z - travel - top15$ >= 0	Further ensures that only neutrino are selected and all muons that enter the analysis are omitted.
Interaction type	Separates the neutral and charged current interactions
Neutrino type	Distinguishes between the neutrino and anti neutrino.

All the values of energy and zenith angle are reconstructed. The process of such reconstruction involves several different steps of processing and reduction. The process starts with selecting 'interesting events'(trigger). The trigger decides which real time data is to be saved based on how its tuned for a particular experimental analysis. The trigger is followed by event reconstruction method that identifies the type of particle (electron neutrino, muon neutrino, muon etc) on each track, and reconstruct their trajectories into tracks. Finally another cleaning-out process selects events based on the selection cuts that are estimated through the known physics calculations.

4.1.1 Reconstructed Energy and Zenith

The reconstructed energy value between 6.31 and 158.49 GeV is used. The detector is not very sensitive for neutrinos below 5 GeV. While above 160 GeV the atmospheric neutrino flux falls significantly and the event statistics available is therefore minimal.

In the figure 6, reconstructed energy values for the charged current interaction of the three flavours of neutrinos and anti neutrinos are shown. The muon neutrino rate is the highest across the entire energy spectrum, while the tau neutrino rate is lowest. In the atmospheric cosmic ray cascade no tau neutrinos are produced. Any rate of tau neutrinos that appears here is due to oscillation of electron and muon neutrinos into tau neutrinos.

The cosine(zenith-angle) distribution for all three flavors that pass through the earth {that is the cos(zenith) between -1 to -0.1; -1 corresponds to neutrinos that comes directly from the 'centre' of earth} and identified through the charged current interactions is given in figure 7. The reconstructed muon and electron neutrino rate is consistent across all the values. While the tau neutrino values are highest when for the track that passes directly through the core of the earth and then decreases consistently. Majority of tau neutrinos that appear through oscillation, is when the neutrinos pass through the core (wherein the matter effects are significantly high, see the figure 3 also in matter effect section).

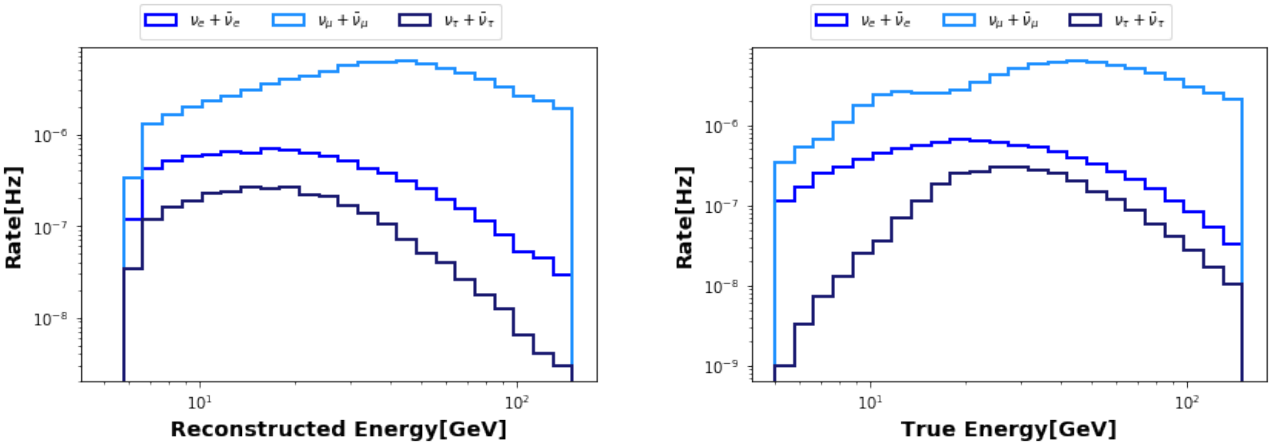

Figure 6: The reconstructed and true energy distributions for all three flavors of neutrinos identified by charged current interaction

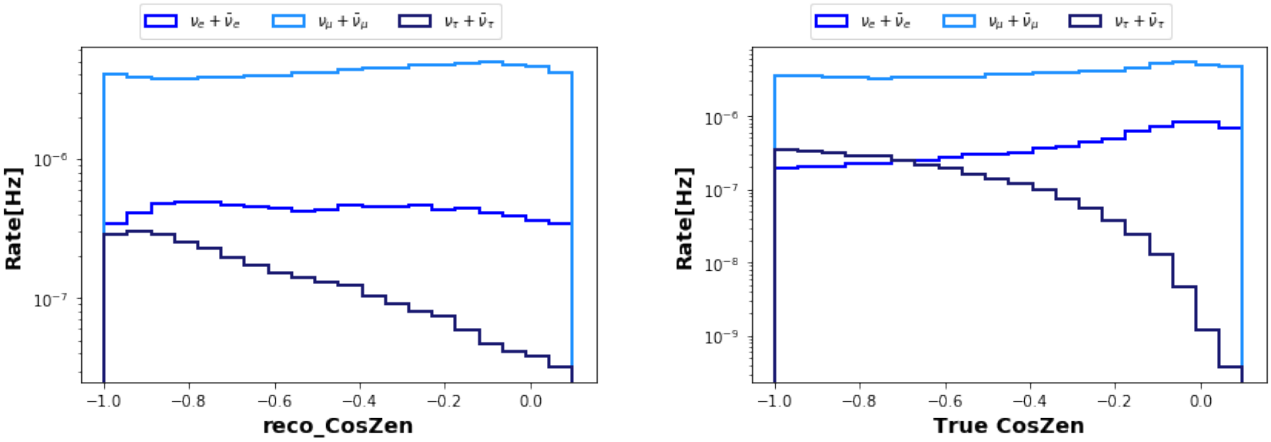

Figure 7: The reconstructed and true cosine(zenith) angle distributions for all three flavors of neutrinos identified by charged current interaction

The figure number 8,9,10 shows the 2D histograms of electron, muon, and tau neutrinos binned in energy and cos(zenith). The maximum number of electron neutrinos populate the low energy range (where the icecube deepcore detector is not yet sensitive enough). Similar observation can be applied to the tau+antitau neutrinos. Moreover these is no flux of tau+anti-tau neutrinos in beyond 40 GeV and above 2 radian zenith angle.

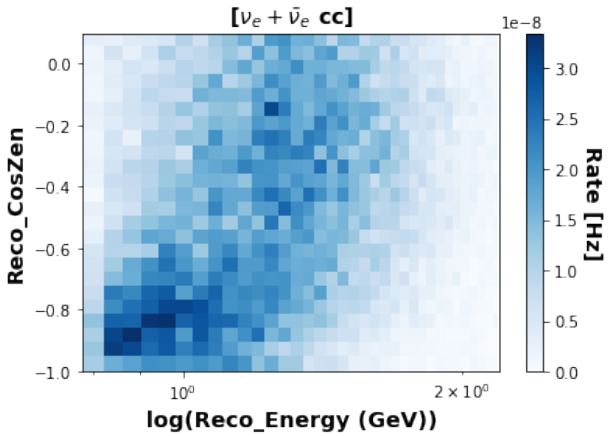

Figure 8: Electron and anti-electron charged current interaction rates

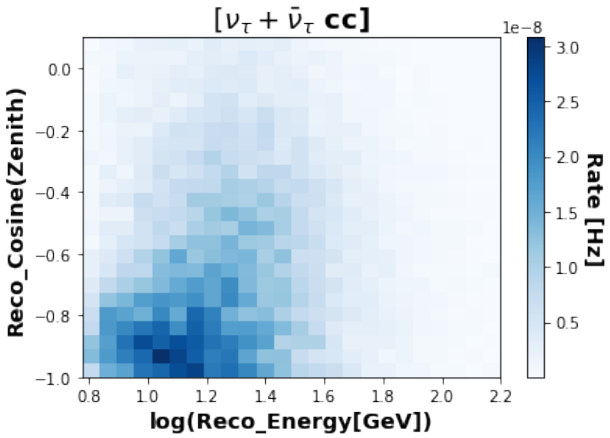

Figure 9: Tau and anti-tau neutrinos charged current interaction rates

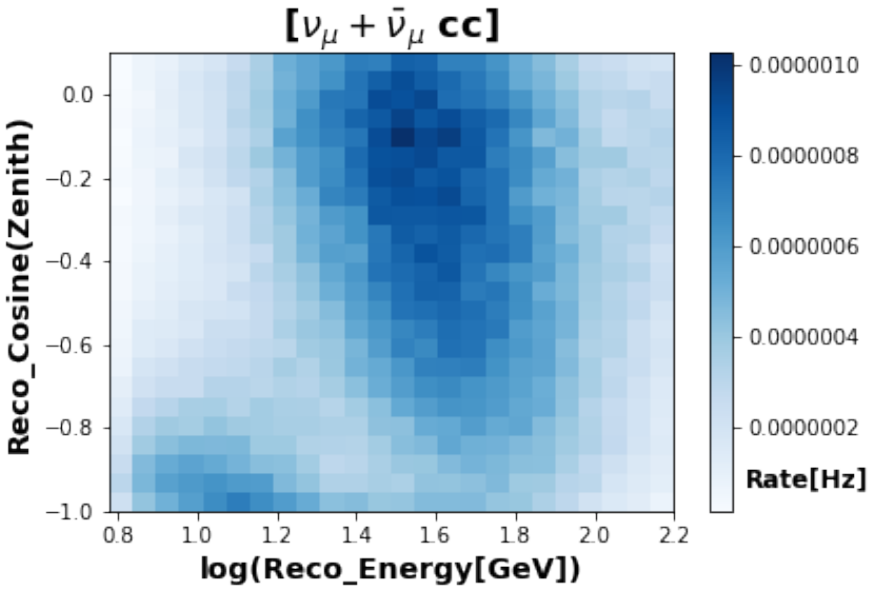

Figure 10: Muon and anti-muon neutrinos charged current interaction rates

For the muon antimuon neutrinos a clear region of $\nu_\mu + \bar{\nu}_\mu$ disappearance between 5 to 40 GeV energy can be identified. The muon neutrino flux peaks at around 40 GeV and at zenith angle little higher than $\frac{\Pi}{2}$. In summary the muon neutrino disappearances the only factor that can be precisely identified. The ongoing update to the deep core detector will increase the sensitivity in an energy region of around 2 GeV, making it more sensitive to probe the tau neutrino appearance. Although the cascade like structure of tau and electron neutrino would indeed make it difficult to separate these two flavors.

4.1.2 GBM-PID Selection

The GBM-PID determines whether an event is track-like from a particle-ID (PID) number. The monte-carlo in this case identifies the track-like signatures for an event. The variable takes values between 0 and 1. Where 0 is for not at all track-like signal while value equal to 1 represents a perfect track. Events which are not reconstructed are given GBM-PID value equal to -1 and automatically omitted in the analysis. For the analyses discussed before this section, GBM-PID values > 0.55 were used. The following are the reconstructed energy and zenith distribution for other GBM-PID values, i.e GBM-PID ¿ 0.35, ¿0.75 and ¿0.97.

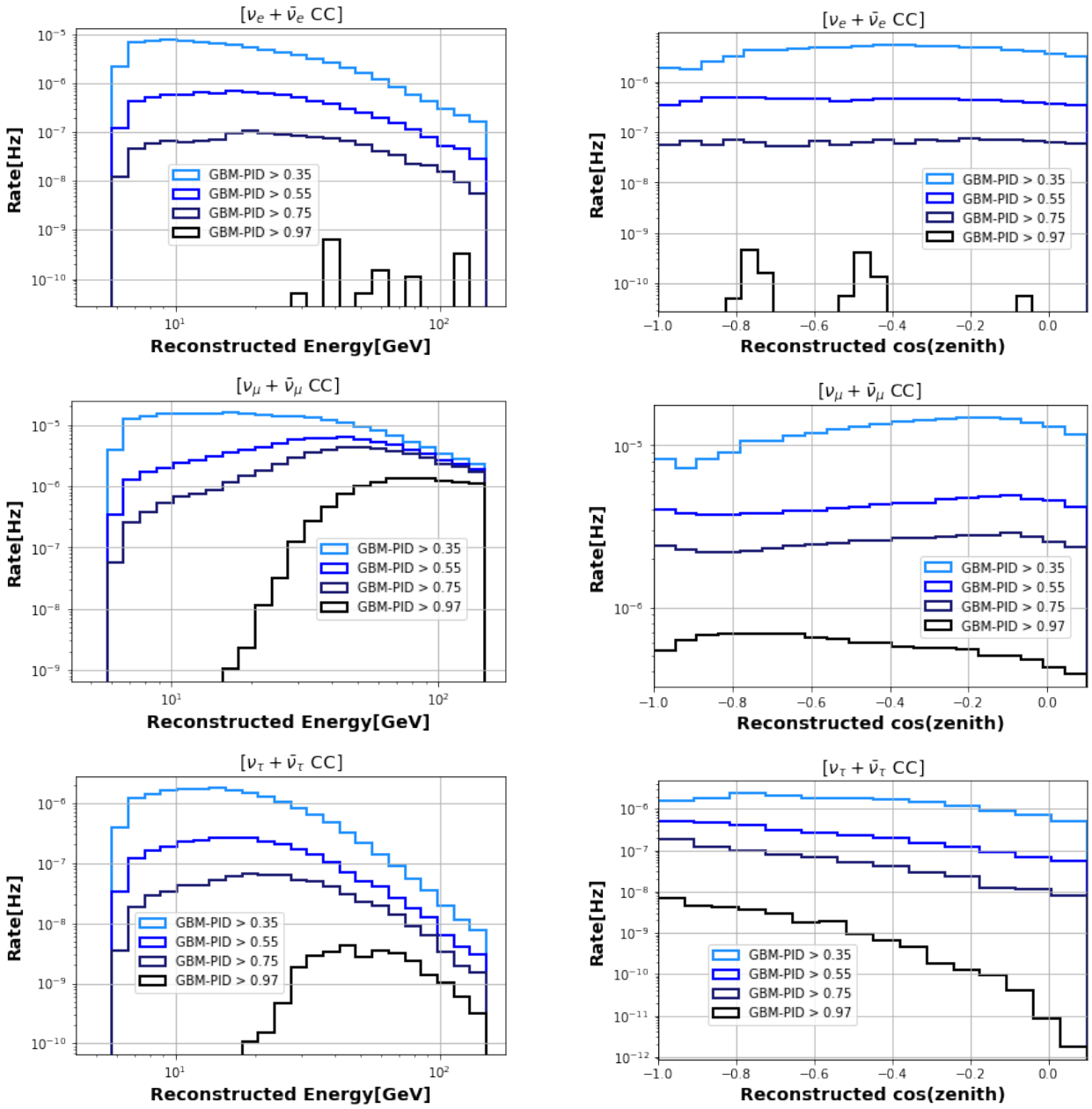

Figure 11: Different GBM-PID selection cuts for three neutrino flavors

From the left panel figures in Figure 11 it can be observed that the most track-like signatures (GBM-PID > 0.97), are not identified in the low energy range (below 25 GeV). The energy rate with other three GBM-PID cuts are more consistent across the spectrum. The distribution across the zenith-angle spectrum is more or less similar, although the rate(the number of events) decreases in an expected manner.

The following figure (Figure 12) shows the 2D histograms for muon and antimuons for four different values of GBM-PID selection. Nothing similar to the $\nu_m u + \bar{\nu}_\mu$ dissapearance valley that appears in the default GBM PID (> 0.55) can be observed in other distributions. There is a large shift (20 GeV) in the peak rate value when all events with GBM-PID ¿ 0.35 are considered. There is not much change between GBM PID > 0.55 and > 0.75, except at the lower energies. For the most track-like events of GBM-PID > 0.97, the low energy neutrinos completely disappear. The most trac-like signatures are therefore obtained only at energy higher than 40 GeV.

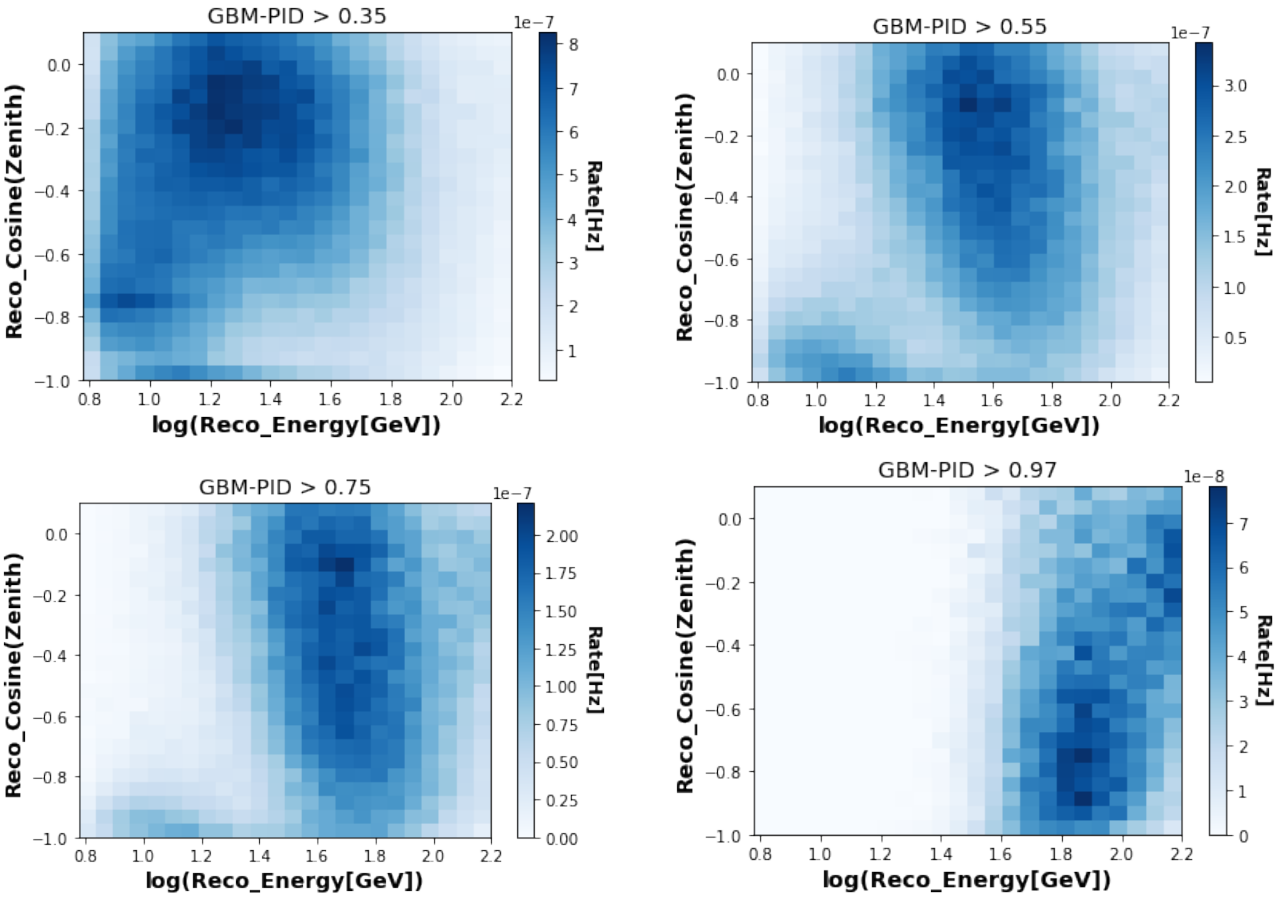

Figure 12: 2D-histograms with different GBM-PID selections for $\nu_\mu + \bar{\nu}_\mu$ neutrinos

5 Conclusion

The distributions of reconstructed energy and reconstructed zenith angle along with the selection cuts used to obtain the data for analysis is shown and discussed and applied to identify the regions of neutrino appearance and disappearance. In the atmospheric neutrinos the initial neutrino flux majorly contains muon and electron neutrino, while the tau neutrino flux is negligible. The simulated data shows the peak in rate of tau neutrinos at about 15 GeV and at zenith angle close to the core of earth. This energy range being slightly above the ice-cube's lower threshold of 5 GeV, tau neutrinos should be visible in the region. The valley of disappearance of the muon neutrinos in the energy range of 10 to 30 GeV is also another important factor to be observed, the same region also corresponds to peak tau neutrino events. The importance of each of the selection criteria is discussed. The results with varying GBM-PID selection cuts are also presented. The simulated event sample that we looked at will be used to compare to data and to extract the newest neutrino oscillation parameter results from 10 years of icecube data.

References

[1] M. G. Aartsen et al. "Determining neutrino oscillation parameters from atmospheric muon neutrino disappearance with three years of IceCube DeepCore data". In: *Physical Review D* 91.7 (Apr. 2015). ISSN: 1550-2368. DOI: 10.1103/physrevd.91.072004. URL: http://dx.doi.org/10.1103/PhysRevD.91.072004.

[2] M. G. Aartsen et al. "Measurement of atmospheric tau neutrino appearance with IceCube DeepCore". In: *Physical Review D* 99.3 (Feb. 2019). ISSN: 2470-0029. DOI: 10.1103/physrevd.99.032007. URL: http://dx.doi.org/10.1103/PhysRevD.99.032007.

[3] Q. R. Ahmad et al. "Measurement of the Rate of $\nu_e + d \rightarrow p + p + e^-$ Interactions Produced by ^8B Solar Neutrinos at the Sudbury Neutrino Observatory". In: *Phys. Rev. Lett.* 87 (7 July 2001), p. 071301. DOI: 10.1103/PhysRevLett.87.071301. URL: https://link.aps.org/doi/10.1103/PhysRevLett.87.071301.

[4] Bruce T. Cleveland et al. "Measurement of the Solar Electron Neutrino Flux with the Homestake Chlorine Detector". In: *The Astrophysical Journal* 496.1 (Mar. 1998), pp. 505–526. DOI: 10.1086/305343. URL: https://doi.org/10.1086/305343.

[5] C. L. Cowan et al. "Detection of the Free Neutrino: a Confirmation". In: *Science* 124.3212 (1956), pp. 103–104. ISSN: 0036-8075. DOI: 10.1126/science.124.3212.103. eprint: https://science.sciencemag.org/content/124/3212/103.full.pdf. URL: https://science.sciencemag.org/content/124/3212/103.

[6] Y. Fukuda et al. "Evidence for Oscillation of Atmospheric Neutrinos". In: *Phys. Rev. Lett.* 81 (8 Aug. 1998), pp. 1562–1567. DOI: 10.1103/PhysRevLett.81.1562. URL: https://link.aps.org/doi/10.1103/PhysRevLett.81.1562.

[7] Takaaki KAJITA. "Atmospheric neutrinos and discovery of neutrino oscillations". In: *Proceedings of the Japan Academy, Series B* 86.4 (2010), pp. 303–321. DOI: 10.2183/pjab.86.303.

[8] Wing Yan Ma. "Physics Potential of the IceCube Upgrade". In: *Journal of Physics: Conference Series* 1468 (Feb. 2020), p. 012169. DOI: 10.1088/1742-6596/1468/1/012169. URL: https://doi.org/10.1088/1742-6596/1468/1/012169.

[9] Ziro Maki, Masami Nakagawa, and Shoichi Sakata. "Remarks on the Unified Model of Elementary Particles". In: *Progress of Theoretical Physics* 28.5 (Nov. 1962), pp. 870–880. ISSN: 0033-068X. DOI: 10.1143/PTP.28.870. eprint: https://academic.oup.com/ptp/article-pdf/28/5/870/5258750/28-5-870.pdf. URL: https://doi.org/10.1143/PTP.28.870.

[10] Wolfgang Pauli. "Pauli letter collection: letter to Lise Meitner". Typed copy. URL: https://cds.cern.ch/record/83282.

[11] B. Pontecorvo. "Neutrino Experiments and the Problem of Conservation of Leptonic Charge". In: *Zh. Eksp. Teor. Fiz.* 53 (1967), pp. 1717–1725.

[12] Christopher Wiebusch. *Physics Capabilities of the IceCube DeepCore Detector*. 2009. arXiv: 0907.2263 [astro-ph.IM].

[13] L. Wolfenstein. "Neutrino oscillations in matter". In: *Phys. Rev. D* 17 (9 May 1978), pp. 2369–2374. DOI: 10.1103/PhysRevD.17.2369. URL: https://link.aps.org/doi/10.1103/PhysRevD.17.2369.